Reduced repressive epigenetic marks, increased DNA damage and Alzheimer's disease hallmarks in the brain of humans and mice exposed to particulate urban air pollution

Lilian Calderón-Garcidueñas[a,b], Andrea Herrera-Soto[c], Nur Jury[c,d], Barbara A. Maher[e], Angélica González-Maciel[f], Rafael Reynoso-Robles[f], Pablo Ruiz-Rudolph[g], Brigitte van Zundert[c,d,**], Lorena Varela-Nallar[c,*]

[a] Universidad Del Valle de México, 14370, Mexico
[b] University of Montana, Missoula, MT, 59812, USA
[c] Instituto de Ciencias Biomédicas (ICB), Facultad de Medicina y Facultad de Ciencias de La Vida, Universidad Andres Bello, Echaurren 183, 8370071, Santiago, Chile
[d] Centro de Envejecimiento y Regeneración (CARE-UC), Facultad de Ciencias Biológicas, P. Universidad Católica de Chile, Alameda 340, 8330036, Santiago, Chile
[e] Centre for Environmental Magnetism and Palaeomagnetism, Lancaster Environment Centre, University of Lancaster, Lancaster, LA1 4YQ, United Kingdom
[f] Instituto Nacional de Pediatría, 04530, Mexico
[g] Programa de Salud Ambiental, Instituto de Salud Poblacional, Facultad de Medicina, Universidad de Chile, Independencia 939, 8380453, Independencia, Santiago, Chile

ARTICLE INFO

ABSTRACT

Exposure to air pollutants is associated with an increased risk of developing Alzheimer's disease (AD). AD pathological hallmarks and cognitive deficits are documented in children and young adults in polluted cities (e.g. Metropolitan Mexico City, MMC). Iron-rich combustion- and friction-derived nanoparticles (CFDNPs) that are abundantly present in airborne particulate matter pollution have been detected in abundance in the brains of young urbanites. Epigenetic gene regulation has emerged as a candidate mechanism linking exposure to air pollution and brain diseases. A global decrease of the repressive histone post-translational modifications (HPTMs) H3K9me2 and H3K9me3 (H3K9me2/me3) has been described both in AD patients and animal models. Here, we evaluated nuclear levels of H3K9me2/me3 and the DNA double-strand-break marker γ-H2AX by immunostaining in post-mortem prefrontal white matter samples from 23 young adults (age 29 $\pm$ 6 years) who resided in MMC (n = 13) versus low-pollution areas (n = 10). Lower H3K9me2/me3 and higher γ-H2A.X staining were present in MMC urbanites, who also displayed the presence of hyperphosphorylated tau and amyloid-β (Aβ) plaques. Transmission electron microscopy revealed abundant CFDNPs in neuronal, glial and endothelial nuclei in MMC residents' frontal samples. In addition, mice exposed to particulate air pollution (for 7 months) in urban Santiago (Chile) displayed similar brain impacts; reduced H3K9me2/me3 and increased γ-H2A.X staining, together with increased levels of AD-related tau phosphorylation. Together, these findings suggest that particulate air pollution, including metal-rich CFDNPs, impairs brain chromatin silencing and reduces DNA integrity, increasing the risk of developing AD in young individuals exposed to high levels of particulate air pollution.

1. Introduction

Urban air pollution is a worldwide environmental health problem affecting millions of people. Epidemiological studies in developed and developing nations have linked exposure to air pollutants, particularly ultrafine (PM$_{0.1}$) and fine particulate matter (PM$_{2.5}$), to increased morbidity and mortality (Cohen et al., 2017) and to diverse neuropathological and neurological abnormalities, including brain cancer (Weichenthal et al., 2019) and impaired cognitive abilities (Calderón-Garcidueñas et al., 2008a, 2019; Chen et al., 2017a; Forns et al., 2017; Harris et al., 2015; Perera et al., 2006; Suglia et al., 2008; Zhang et al., 2018). Moreover, traffic-derived air pollutants, residency close to heavily trafficked roads and exposure to high concentrations of PM$_{2.5}$ have been associated with increased risk of dementia and

---

Alzheimer's disease (AD) (Calderón-Garcidueñas et al., 2004; Chen et al., 2017b; Jung et al., 2015; Zhang et al., 2018). Children and young adults from Metropolitan Mexico City (MMC) exposed to moderate $PM_{2.5}$ levels exhibit neuropathological hallmarks of AD, including hyperphosphorylated tau and amyloid-β (Aβ) plaques (Calderón-Garcidueñas et al., 2008b, 2012, 2018). Abundant magnetite and other co-associated metal-rich combustion- and friction-derived nanoparticles (CFDNPs) have been detected in brains of children and young adult MMC residents (Maher et al., 2016), showing that air pollution particles can translocate to the human brain.

Recently, epigenetic gene regulation has emerged as a potential mechanism linking pollution and disease outcomes including heart disease, cancer and asthma (Li et al., 2018; Vecoli et al., 2016; Yang et al., 2017). Epigenetic mechanisms organize chromatin structure to regulate changes in gene activity. Epigenetic gene regulation can be mediated through DNA methylation, histone post-translational modifications (HPTMs), exchange of histone variants, and nucleosome remodeling. HPTMs are key components for defining chromatin status as they can either promote or inhibit transcription, depending on the modification and on the modified histone residue. It is notable that deregulation of epigenetic control is a common feature of a number of diseases, including brain disorders (Berson et al., 2018; Frost et al., 2014; Graff and Tsai, 2013; Klein et al., 2019). Specifically, recent analysis of tissue derived from AD patients and tau animal models indicate that a widespread loss of the repressive HPTMs, H3K9me2 and H3K9me3 (H3K9me2/me3) may underlie DNA damage and altered gene expression in AD (Frost et al., 2014; Mansuroglu et al., 2016).

Whether from fission yeast to humans, H3K9me2/me3 deposits are required to transcriptionally silence tissue-specific and developmental stage-specific coding genes in euchromatic and facultative heterochromatic (fHC) regions, typically to ensure lineage specificity (Allis and Jenuwein, 2016; Bannister and Kouzarides, 2011; Bustos et al., 2017; Saksouk et al., 2015; Trojer and Reinberg, 2007; Zeller and Gasser, 2017). Additionally, H3K9me3 is enriched at constitutive HC (cHC) regions which comprise diverse repeat element classes, including tandem repeats and transposable elements (Dumbovic et al., 2017; Harr et al., 2016; Zeller and Gasser, 2017). H3K9me2 is also found at cHC regions; however, this mark is particularly enriched at minor satellites of centromeric regions (Allis and Jenuwein, 2016; Peters et al., 2001; Saksouk et al., 2015; Trojer and Reinberg, 2007; Zheng et al., 2019).

Here we analyzed the repressive H3K9me2/me3 marks in postmortem frontal white matter samples of young adults from MMC that exhibit AD hallmarks and abundant CFDNPs in the brain. Frontal white matter samples from low-pollution areas were used as controls. In addition, frontal cortex samples of mice chronically exposed to urban air pollution or HEPA-filtered air were also examined.

2. Materials and methods

2.1. Human brain samples

The autopsy frontal samples were obtained from forensic cases from 23 individuals (Table 1) with no identifiable personal data, not meeting the regulatory definition of human subject research. The cohorts were selected from the MMC area (high pollution-exposure area, above USA EPA and WHO $PM_{10}/PM_{2.5}$ standards), and from control locations consisting of small cities in Mexico that have less than 75,000 inhabitants and levels for criteria air pollutants (ozone, particulate matter, sulfur dioxide, nitrogen oxides and carbon monoxide) below the current USA EPA standards (Calderón-Garcidueñas et al., 2016). The age range of all individuals was from 20 to 40 years old. The mean age of the 10 control individuals was 29.3 years old, and for the 13 MMC individuals, 29.8 years. Detection of Htau Stage and Aβ Phase was carried out as previously described (Calderón-Garcidueñas et al., 2018).

2.2. Light microscopy and transmission electron microscopy (TEM)

TEM and 1 μm toluidine blue sections were performed in 14 frontal samples: control n = 5, age 29.4 ± 6.5 years and MMC n = 9, age 30.3 ± 7.43 years (Table 1). One-micron toluidine blue sections and ultrastructural features in frontal samples were assessed by experienced pathologists and electron microscopists, blind to the study group. Sections were stained with uranyl acetate and lead citrate and examined with a JEOL JEM-1011 TEM microscope. EM evaluations were made from photomicrographs with final magnifications at 1,300x, 3,000x, 25,000x, 50,000x and 80,000x. Nanoparticle (NP) numbers were counted in the nuclei of neurons in both control and exposed cohorts. NP numbers were counted in 20 neuronal (frontal) nuclei from each subject, at a magnification of 83,300x, with an area of 34.37 μm in each image. We counted NPs which were ≥10 nm in diameter.

2.3. Measurements of magnetic remanence

Magnetic measurements were made at the Centre for Environmental Magnetism and Paleomagnetism, Lancaster University. To quantify the ferrimagnetic content of the frontal cortex sample, we freeze-dried the sample for 24 h, applied a direct current field of 1 T and measured the saturation magnetic remanence (SIRM) with a cryogenic magnetometer (GM400, mean background noise level 5.9×10^{-11} Am^2; Cryogenic Consultants Ltd.) at room and low temperature (77 K). To estimate the ferrimagnetic concentration per 1 g of dry tissue weight, we divided the measured $SIRM_{77 K}$ by an empirically-derived value for $SIRM_{SP/SD}$ magnetite of 13.8 $Am^2·kg^{-1}$. This value is appropriate for the interacting, mixed single domain (SD) and superparamagnetic (SP) magnetite particles observed in human brain tissue, of mean particle size ~31 nm (Maher, 1988; Maher et al., 2016), rather than the 'conventional' $SIRM_{magnetite}$ value of 46 $Am^2·kg^{-1}$, which is applicable only to pure, non-interacting, single domain (50 nm) magnetite particles. The number of magnetite particles/g dry tissue was then estimated by dividing the mass of magnetite (again, per 1g dry tissue weight), by the mass of 1 magnetite particle (8.07224^{-11} μg).

2.4. Animals

Two-month-old C57BL/6J female mice purchased from the Jackson laboratory (Maine, USA) were used. All protocols involving mice were carried out according to NIH guidelines as well as ARRIVE guidelines, and were approved by the Ethical and Bio-security Committees of Universidad Andrés Bello.

2.5. Model of real-world exposure to urban air pollution

Our experimental design consisted of two closed, isolated, temperature-regulated chambers, each containing three shelves, located outdoors on the University Andres Bello Campus República in downtown Santiago (Chile). Four female wild-type C57BL/6J mice were housed per cage (N = 4 per experimental group) in a 12-h light/dark cycle. The "Pollution group" received direct air from the outdoor environment, while the "Filtered Air group" had a BioMAX™ HEPA filter (model FH12126) located before the air entry. Air quality was monitored using a DustTrak II Aerosol monitor for $PM_{2.5}$ and a P-TRAK ultrafine particle counter for UFP (model 8532 and 8525, respectively, TSI incorporated, Shoreview, MN). $PM_{2.5}$ measurements were compared, and adjusted, with the closest monitoring station of "Parque O'Higgins" (http://sinca.mma.gob.cl), as previously described (Suarez et al., 2014). Animals were purchased from Jackson Laboratory (Maine, USA) and arrived in Chile when they were 2 months old; they were immediately and randomly separated into two groups, and maintained in their respective chambers from May to November, the winter months when pollution is highest in Santiago (Fig. S1).

Table 1
Cumulative PM$_{2.5}$ and autopsy data in controls and MMC subjects.

Samples	Age (years)	Gender[b]	Cause of death[c]	CPM$_{2.5}$[d] ($\mu g/m^3$)	HTau[e]	Aβ Phase[f]	Electron Microscopy
Control							
C1	21	F	0	< 100	0	0	Yes
C2	24	F	0	< 100	0	0	
C3	25	M	0	< 100	0	0	Yes
C4	26	F	0	< 100	0	0	
C5	30	M	0	< 100	0	0	Yes
C6	30	M	0	< 100	0	0	
C7	32	M	0	< 100	0	0	
C8	34	M	0	< 100	0	0	
C9	34	M	2	< 100	0	0	Yes
C10	37	M	0	< 100	0	0	Yes
MMC							
P1	20	M	1	457	2	2	Yes
P2	22	M	1	634	2	2	Yes
P3	23	M	2	605	2	2	Yes
P4	23	M	0	399	2	2	
P5	24	M	2	707	2	2	
P6[a]	26	M	2	508	2	2	Yes
P7	32	M	2	570	2	2	
P8	35	M	0	881	2	2	Yes
P9	35	M	0	2238	5	3	Yes
P10	36	M	2	940	3	2	
P11	36	M	1	570	5	3	Yes
P12	38	M	1	899	4	3	Yes
P13	38	M	1	583	3	2	Yes

[a] Saturation remanent magnetization (77 K) of $17.2 \times 10^{-6} Am^2 kg^{-1}$, equivalent to a magnetite concentration of 1.2 $\mu g/g$ dry frontal tissue and particle numbers of ~15 billion NPs/g of freeze-dried tissue.

[b] Gender: F = female, M = male.

[c] Cause of death: 0 = accidents, 1 = homicides, 2 = suicides.

[d] CPM$_{2.5}$: Cumulative PM$_{2.5}$ for each subject, calculated based on age at death (including pregnancy time) and annual average PM$_{2.5}$ concentrations of their urban residency.

[e] Htau Stage: 0 = absent, 1 = pretangle stages a-c, 2 = pretangle stages 1a, 1b, 3 = NFT stages I, II, 4 = NFT stages III-IV, 5 = NFT stages V-VI

[f] Aβ Phase:0 = absent, 1 = basal temporal neocortex, 2 = all cerebral cortex, 3 = subcortical portions forebrain, 4 = mesencephalic components, 5 = Reticular formation and cerebellum.

2.6. Immunostaining

For human samples, paraffin embedded tissue blocks were sectioned at a thickness of 8 μm. Tissue sections were deparaffinized and rehydrated in a graded alcohol series (100%, 96%, 70% and 50%) for 10 min in each bath and rinsed in running tap water before pre-treatment with sodium citrate buffer 0.01M, pH 6 for 20 min for antigen retrieval. For mouse samples, after trans-cardiac perfusion with saline solution, the brain was removed, hemispheres were immersed in 4% paraformaldehyde overnight, cryoprotected in 10–30% sucrose gradient over 3 days, embedded in optimal cutting temperature medium (OCT), and sagittal slices cut at 40 μm on a cryostat. For the immunohistochemistry protocol, samples were washed 3 times for 5 min each, in a solution of 0.01M PBS 0.15% Triton X-100 and incubated with 0.3% H_2O_2 at room temperature for 30 min, then incubated for 1h with blocking solution containing 5% BSA in 0.01M PBS 0.15% Triton X-100, and incubated overnight at 4 °C with the primary antibodies diluted in blocking solution. Primary antibodies used were: mouse anti-H3K9me2 (1:500, Abcam, ab1220), rabbit anti-H3K9me3 (1:400, Abcam, ab8898), rabbit anti-H3K4me3 (1:500, Abcam, ab8580), rabbit anti-H3K36me3 (1:500, Abcam, ab9050), mouse anti-γ-H2A.X (1:1,000, Abcam, ab22551), mouse anti-NeuN (1:600, Merck Millipore, mab377). After being rinsed 3 times with 0.01M PBS 0.15% Triton X-100, sections were incubated for 1 h with biotinylated secondary antibodies (mouse biotinylated antibody BA-9200 1:250, and rabbit biotinylated antibody 1:250, Vectastain, ABC Elite kit PK-6101, Vector Laboratories) diluted in blocking solution, followed by 1 h incubation with avidin–biotin–peroxidase complex (1:125, Vectastain, ABC Elite kit PK-6101, Vector Laboratories). Finally, a 30% H_2O_2 solution was added in the presence of 3,3′-diaminobenzidine (DAB, 1 mg/ml) to visualize the antigen–antibody complex. Staining for hematoxylin and eosin was performed in tissue slices sectioned at a thickness of 3 μm according to a routine protocol in one set of all individuals' biopsies, in order to identify the different regions of interest in this study.

For the immunofluorescence protocol, mouse tissue sections were permeabilized with 0.5% Tritón-X100 and incubated for 4 h with blocking solution containing 3% BSA plus 3% donkey serum in 0.01M PBS 0.5% Triton X-100, and incubated overnight at 4 °C with the primary antibodies diluted in blocking solution. Primary antibodies used were: mouse anti-H3K9me2 (1:1,000, Abcam, ab1220), rabbit anti-H3K9me3 (1:1,000, Abcam, ab8898), mouse anti-NeuN (1:300, Millipore, mab377), and rabbit anti-NeuN (1:300, Millipore, ABN78). After being rinsed 3 times with 0.01M PBS 0.5% Triton X-100, sections were incubated for 2 h at room temperature with secondary donkey Alexa-conjugated antibodies (1:500, Molecular Probes). TO-PRO-3 (1:1,000, Life Technologies, T3605) was used as a nuclear dye. The sections were imaged on a Confocal Leica SP8 microscope.

2.7. Quantification of immunostaining

For the immunohistochemistry, all slices were evaluated for DAB staining in the white matter nuclei of the frontal cortex using the quantification method of reciprocal intensity (Nguyen et al., 2013). Reciprocal intensity directly correlates with an increased staining intensity for the nuclear marks (Nguyen et al., 2013). A uniform sized region of interest (ROI) was used to measure the mean intensity of each stained nucleus using the ImageJ Fiji software. Six images were acquired per subject at 100× magnification (Motic®BA310 Biological Light microscope) and all nuclei per image were quantified, to obtain a mean intensity. For immunofluorescence staining, the fluorescence intensity was measured in a ROI covering the entire nuclear area (delineated by TO-PRO-3 staining). At least 20 NeuN positive cells per image

were analyzed. A total of 3 images were quantified per animal using the ImageJ Fiji software.

2.8. Immunoblot analysis

Cortex tissue samples were lysed in ice-cold RIPA buffer containing 25 mM Tris-Cl (pH 7.6), 1% NP-40, 1% sodium deoxycholate, 0.1% SDS, 150 mM NaCl (ThermoScientific, cat: 89,900) and Protease and Phosphatase Inhibitor Mini Tablets (Thermo Scientific, A32961). Protein lysates were centrifuged at 14,000g for 20 min (4 °C). Supernatants were boiled in lithium dodecyl sulfate sample buffer (Thermo-Fisher, NP0007) containing 1% β-mercaptoethanol. Protein samples (30 μg) were resolved by 10% SDS-PAGE, transferred to PVDF membrane (Roche). Membranes were blocked for 1 h with 5% BSA in Tris-buffered saline-0.05% Tween (TBS-T) and incubated overnight (4 °C) with primary antibodies anti-AT8 (Thermo Fisher, MN1020) or anti-Tau-5 (Santa Cruz Biotechnology, sc-58860) in blocking solution. Membranes were rinsed 3 times in TBS-T following by 2 h incubation with HRP-conjugated secondary antibodies and developed using ECL prime (GE Life Sciences, RPN2232). Densitometric analysis was performed using ImageJ software.

2.9. Statistical analysis

Statistical analyses were performed using GraphPad Prism 5. Data are reported as mean ± standard error of the mean (SEM). Mann-Whitney U-tests were used to compare human samples and unpaired Student's t-tests for mouse samples. $p < 0.05$ was considered statistically significant (p-values for all results are indicated in each figure legend).

3. Results

3.1. Lower H3K9me2/me3 staining in nuclei of prefrontal white matter from young adult urbanites chronically exposed to air pollution

We used post-mortem frontal white matter samples from human subjects ranging from 20 to 40 years old. Thirteen of the subjects had lived all their lives in MMC; 10 had resided in low-pollution control areas (Table 1). All MMC subjects were associated with high cumulative PM$_{2.5}$ (CPM$_{2.5}$), estimated from age at death and annual average PM$_{2.5}$ concentrations of their urban residency (Calderón-Garcidueñas et al., 2018, 2019). In addition, all MMC subjects (even the young adults) exhibited hyperphosphorylated tau (pre-tangles or neurofibrillary tangles) and Aβ phases 2–3 (Braak et al., 2011; Braak and Del Tredici, 2015; Thal et al., 2002). Control subjects did not show any of the AD hallmarks.

In all samples, we carried out immunohistochemistry analysis of HPTMs in frontal white matter nuclei. First, we analyzed H3K9me2 (Fig. 1A), a repressive HPTM enriched in coding genes in euchromatic and fHC regions to transcriptionally silence tissue-specific or developmental-stage-specific coding genes, and in cHC predominantly to repress minor satellite repeats within centromeric regions (Allis and Jenuwein, 2016; Saksouk et al., 2015; Trojer and Reinberg, 2007; Zeller and Gasser, 2017). To evaluate the levels of this epigenetic mark, we measured the reciprocal intensity of nuclear staining, which correlates directly with the amount of chromogen present in the sample and therefore with the immunostaining (Nguyen et al., 2013).

Imaging and quantification revealed a significant decrease in the global intensity of H3K9me2 staining in nuclei of brain samples from MMC urbanites compared to controls (Fig. 1A–B). To further characterize H3K9me2 staining in each nucleus, nuclear immunostaining was classified as "light", "medium" or "dark" based on the reciprocal intensity value (Fig. 1C). We evaluated the intensity distribution of all nuclei within the acquired images for each control and polluted subject (Fig. 1D, Fig. S2). A significant increase in the percentage of "light"

stained nuclei, concomitant with a significant decrease in the percentage of "medium" and "dark" stained nuclei, was observed in MMC subjects compared to control urbanites (Fig. 1D).

We also analyzed H3K9me3 (Fig. 2A), another repressive HPTM associated with the silencing of coding genes and repetitive elements, particularly with highly clustered satellite repeat sequences (major satellites in mice and macro satellites in humans) within pericentric cHC regions and with RNA transposons (Allis and Jenuwein, 2016; Saksouk et al., 2015; Zeller and Gasser, 2017). Imaging and quantification showed a significant decrease in global nuclear intensity of H3K9me3 staining in the white matter nuclei of MMC subjects compared to control subjects (Fig. 2A–B). As for H3K9me2, H3K9me3 staining in each nucleus was classified as "dark", "medium" or "light" (Fig. 2C), and nuclei distribution for each subject was classified in these categories (Fig. 2D, Fig. S3). A significant increase in the percentage of "light" or "no staining" nuclei, together with a decrease in the percentage of "medium" stained nuclei, was observed in samples of MMC compared to control samples (Fig. 2D). These results indicate reduced levels of both H3K9me2 and H3K9me3 in white matter nuclei of MMC residents compared to controls, suggesting that chronic exposure to air pollution induces a loss of HPTM-mediated repression in the prefrontal cortex of humans. In addition, we evaluated changes in two HPTMs associated to transcription activation, H3K4me3 and H3K36me3. H3K4me3 is associated with the 5' regions of active genes, and the levels of this modification correlate with transcription rates, active polymerase II occupancy, and histone acetylation (Ruthenburg et al., 2007). H3K36me3 is strongly enriched across the gene body of active genes, and H3K36me3 level correlates with the level of gene transcription (Mikkelsen et al., 2007). Contrary to what was observed for H3K9me2/me3, both activation marks were increased in MMC residents compared to control subjects (Figs. S4 and S5). These results suggest that pollution induces loss of repressive marks and gain of active epigenetic marks in the prefrontal white matter.

3.2. Higher levels of γ-H2A.X in nuclei of prefrontal white matter from urbanites chronically exposed to air pollution

H2A.X, a variant of histone H2A, is a component of the histone octamer in a subset of nucleosomes. When DNA double-strand breaks (DSBs) occur, H2A.X is phosphorylated to form γ-H2A.X, which is central in the protein recruitment and signaling cascade of the DNA damage response (Kinner et al., 2008). γ-H2A.X detection is a quantitative method for detection of even low-levels of DSBs (Rogakou et al., 1999; Rothkamm and Lobrich, 2003; Sedelnikova et al., 2002), thus it is used as a biomarker for DSBs and DNA damage (Ivashkevich et al., 2012). We evaluated by immunohistochemistry the presence and levels of γ-H2A.X in white matter nuclei from subjects from MMC and low-pollution areas (Fig. 3A). Imaging and quantification of the reciprocal intensity revealed a significant increase in nuclear intensity of γ-H2A.X staining in subjects from MMC compared to controls (Fig. 3A–B). As for the H3K9me2/me3 analyses, γ-H2A.X nuclear staining was classified as "dark", "medium" or "light" based on the reciprocal intensity value (Fig. 3C). Nuclei from MMC subjects displayed increased levels of "dark" staining compared to controls (Fig. 3D, Fig. S6). Moreover, there was a significant decrease in the percentage of nuclei with "light" or "no staining" concomitantly with a significant increase in the percentage of "dark" nuclei in samples from MMC subjects compared to controls (Fig. 3D). These results show that there are increased levels of DSBs in white matter nuclei of MMC subjects, suggesting that chronic exposure to air pollution may increase DNA damage in human brains.

3.3. Presence of CFDNPs in neuronal, glial and endothelial nuclei of prefrontal samples from urbanites chronically exposed to air pollution

We focused on identifying NPs with the characteristics of solid CFDNPs which occur in abundance in urban, especially roadside
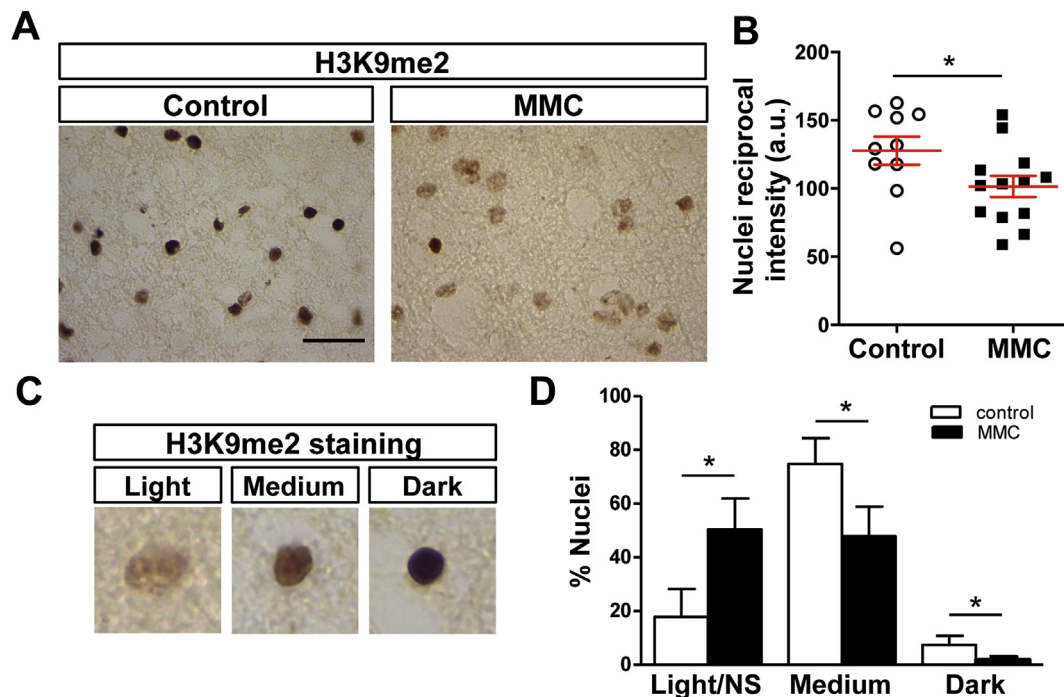
Fig. 1. Immunodetection of H3K9me2 in prefrontal white matter nuclei from control and MMC urbanites. (A) Representative immunostaining of H3K9me2 in white matter of prefrontal tissue sections from residents from MMC and from low-pollution areas as controls. Scale bar: 20 μm. (B) Quantification of reciprocal intensity of H3K9me2 staining in white matter nuclei from each individual control and MMC samples is indicated along with mean ± SEM. *p = 0.04, Mann-Whitney *U* test (control: N = 10 subjects; MMC: N = 13 subjects). (C) Representative nuclei positive for H3K9me2 staining categorized as "light", "medium" or "dark" based on the reciprocal intensity value, which correlates with the amount of chromogen present in the sample (light: 0–99; medium: 100–174; dark: 175–250). (D) Percentage of white matter nuclei of subjects in each of the categories described in C, or with "no staining" (NS) which was added to the percentage of "light staining". *p = 0.04 for all categories (MMC versus control), Mann-Whitney *U* test (control: N = 10 subjects; MMC: N = 13 subjects).

environments: rounded, electrodense (typically metal-bearing) NPs which reflect their formation at high temperatures (i.e. > ~100 °C) and their subsequent rapid cooling and/or partial oxidation upon atmospheric emission (Maher et al., 2016; Maher, 2019). Such NPs were identified in nuclei of neuronal, glial and endothelial cells in prefrontal cortex samples from control and MMC subjects using transmission electron microscopy (TEM) (Fig. 4). While CFDNPs were observed in samples from control (Fig. 4A) and MMC subjects (Fig. 4B–E), the numbers of these NPs were higher in nuclei of MMC subjects. Quantitative analysis revealed a significant increase in the number of CFDNPs in the nuclei of frontal neurons from MMC residents (28 ± 9) compared to controls (9 ± 2) and (p < 0.001); the NPs size range was 10–48 nm, average 26.7 ± 11.6 nm.

Additionally, we measured the saturation magnetic remanence (SIRM) of an MMC frontal tissue sample (at 77 K) in order to quantify the concentration and particle numbers of ferrimagnetic grains (> ~20 nm) (Maher et al., 2016). Such strongly magnetic NPs are ubiquitously and abundantly present in airborne particulate pollution; produced, for example, from vehicle exhaust emissions and brake-wear (Gonet and Maher, 2019). Magnetite NPs that are strikingly similar to those which characterize airborne particulate pollution have previously been found in varying concentrations in the brains of MMC residents (Maher et al., 2016). This magnetic analysis revealed that MMC subject No.6 (Table 1) had ~1.2 μg magnetite/g of frontal tissue, equivalent to ~ 15 billion magnetite NPs/g of freeze-dried frontal tissue. Together with the TEM observations, these data suggest that the rounded, electrodense NPs found in the frontal cortex of MMC subjects comprise at least in part CFDNPs.

3.4. Mice exposed to particulate air pollution display lower H3K9me2/me3 repressive histone marks and higher γ-H2A.X in the frontal cortex

Accumulating evidence indicates that in addition to environmental factors, epigenetic mechanisms are influenced by lifestyle factors such as diet, physical activity, physiological stress, smoking and alcohol consumption, among others (Alegria-Torres et al., 2011). Therefore, to test whether particulate air pollution can specifically induce alterations in H3K9me2/me3 and γ-H2A.X in an experimental situation, 2-month-old C57BL/6J female mice from Maine (USA; annual mean ≤ 15 μg m^{-3}) were exposed for 7 months to the polluted urban atmosphere of Santiago (Chile). Similar to MMC (Querol et al., 2008), Santiago is characterized by high levels of $PM_{2.5}$ and ultrafine particles (UFPs), mainly contributed by industrial and traffic sources (Jorquera and Barraza, 2012; Prieto-Parra et al., 2017; Suarez et al., 2014).

$PM_{2.5}$ concentrations in Santiago usually exceed daily and annual Chilean norms of 50 μg m^{-3} and 20 μg m^{-3}, respectively (https://sinca.mma.gob.cl/index.php/pagina/index/id/norma; https://www.leychile.cl/Navegar?idNorma=1025202), and international standards and recommendations, such as the WHO air quality guidelines of 25 μg m^{-3} and 10 μg m^{-3} for daily and annual means, respectively (World Health Organization, 2005).

For this experiment, mice were housed in chambers in downtown Santiago either directly exposed to ambient air ('pollution group') or to HEPA-filtered air ('filtered air control group'). The HEPA filters are effective in removing particles but not gases. Airborne PM within the chambers was measured throughout the whole experiment (7 months). As expected, we found high $PM_{2.5}$ (mean > 55 μg m^{-3}) and UFP concentrations (reaching > 26,000 counts·cm^{-3}), during the exposure period in the pollution chamber (Fig. S1). In contrast, the filtered air group was exposed to much lower PM levels, with reductions in $PM_{2.5}$ and UFP exposures of 75% and 65%, respectively (Fig. S1). After 7
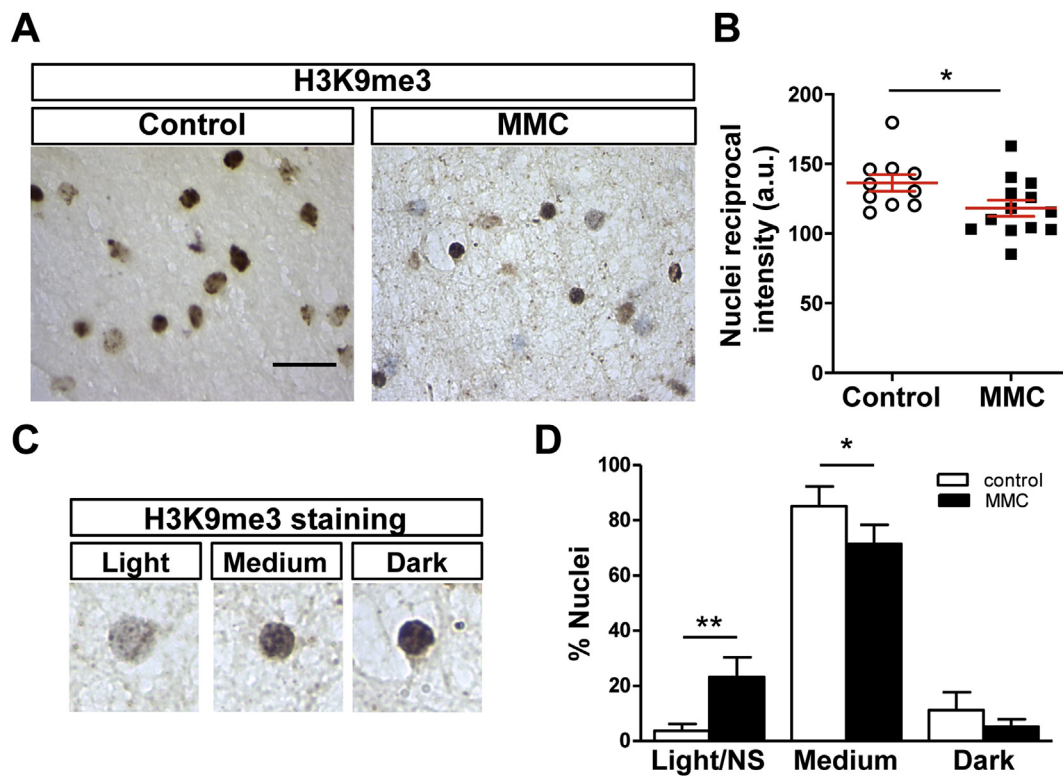
Fig. 2. Immunodetection of H3K9me3 in prefrontal white matter nuclei from control and MMC urbanites. (A) Representative immunostaining of H3K9me3 in white matter of tissue sections from MMC and low polluted areas as control. Scale bar: 20 μm. (B) Quantification of reciprocal intensity of H3K9me3 staining in white matter nuclei from each individual control and MMC sample is indicated along with mean ± SEM. *p = 0.03, Mann-Whitney *U* test (control: N = 10 subjects; MMC: N = 13 subjects). (C) Representative nuclei positive for H3K9me3 staining categorized as "light", "medium" or "dark" based on the reciprocal intensity value, which correlates with the amount of chromogen present in the sample (light: 0–99; medium: 100–174; dark: 175–250). (D) Percentage of white matter nuclei of subjects in each of the categories described in C or with "no staining" (NS) which was added to the percentage of "light" staining. **p = 0.009 (light/NS), *p = 0.05 (medium), MMC versus control, Mann-Whitney *U* test (control: N = 10 subjects; MMC: N = 13 subjects).

months of exposure, animals were sacrificed and sagittal brain slices were examined by immunofluorescence staining to test for H3K9me2/me3 in nuclei positive for the neuronal marker NeuN in the frontal cortex. Imaging and quantification revealed significantly decreased nuclear staining of both H3K9me2 (Fig. 5A–C) and H3K9me3 (Fig. 5D–F) in the nuclei of animals from the pollution group compared to the controls.

Additionally, we used the nuclear staining TO-PRO-3 to gain insights into the chromatin organization within the neurons. DNA fluorescence staining assays, such as TO-PRO-3, NucBlue, DAPI and Hoechst, result in dense structures – "chromocenters" - resembling highly clustered satellite repeat sequences (major satellites in mice and macro satellites in humans) within pericentric cHC regions (Lehnertz et al., 2003; Peters et al., 2003; Saksouk et al., 2015). We found that in control cortical neurons H3K9me3 foci co-localized with the chromocenters concentrated at the nucleolar periphery (Fig. 5D–E), whereas the repressive mark H3K9me2 was dispersed and concentrated in smaller and more blurry foci that did not co-localize with TO-PRO-3-chromocenters (Fig. 5A–C). We did not observe changes in staining patterns and intensity of TO-PRO-3 (Fig. 5A–B and Fig. 5D–E). Imaging and quantification further revealed that the nuclear area was unaltered between the high-pollution and control groups (lower graphs Fig. 5C and F).

Also, we evaluated γ-H2A.X nuclear staining in the frontal cortex of the pollution and filtered air groups by immunohistochemistry (Fig. 5G), which revealed statistically increased levels of γ-H2A.X in pollution-exposed mice compared to controls (Fig. 5H). This result indicates that, concomitantly with the reduction in H3K9me2/me3, there were increased levels of DSBs in the frontal cortex of mice chronically exposed to high levels of particulate air pollution.

3.5. Mice exposed to particulate air pollution display increased levels of tau phosphorylation

Finally, we examined levels of tau phosphorylation at the AT8 phosphoepitope that requires tau protein to be phosphorylated at both serine 202 and threonine 205 (Goedert et al., 1995), in cortical protein extracts from mice exposed to air pollution or filtered air (Fig. 6A). Densitometric analysis revealed that tau protein phosphorylation, measured as AT8 to Tau5 (total tau) immunoreactivity ratio, was higher in frontal cortex from mice exposed to high levels of particulate pollution compared to controls (Fig. 6B). This result indicates that as observed in human samples from MMC subjects, mice exposed to particulate air pollution exhibit AD-related tau phosphorylation.

4. Discussion

Here we found that, compared to low-pollution controls, apparently clinically healthy young urbanites exposed to concentrations of $PM_{2.5}$ above the USA-EPA annual standard exhibit reduced H3K9me2/me3 levels, increased γ-H2A.X levels and much greater abundance of rounded, electrodense NPs (~10–50 nm diameter). At least a fraction of the observed NPs, which occur in the nuclei of neuronal, glial and endothelial cells, is iron-rich and ferrimagnetic in nature and likely derived from combustion and friction processes as previously determined (by high resolution TEM and magnetic remanence measurements) in MMC frontal brain tissue samples (Maher et al., 2016). Our new data support a working model in which the loss of H3K9me2/me3 may cause aberrant gene transcription, genome instability and DNA damage, leading to cognitive impairment as has been evidenced both in patients and tau animal models of AD.
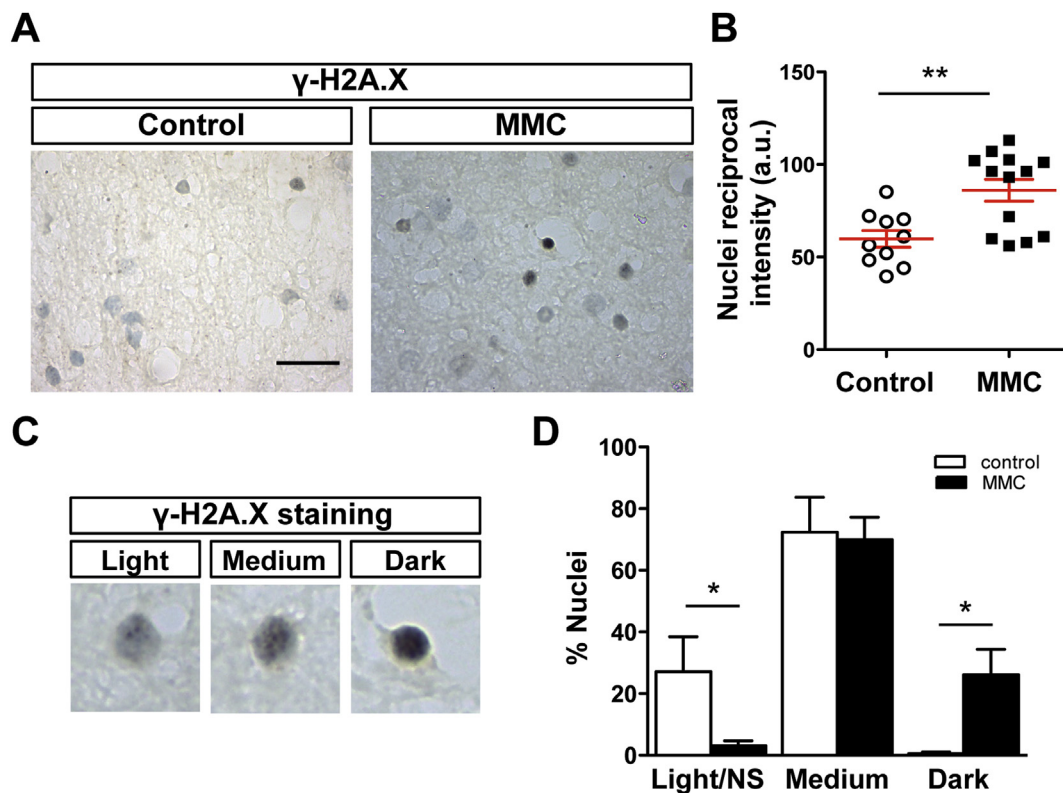
Fig. 3. Immunodetection of γ-H2A.X in nuclei of prefrontal white matter from control and MMC urbanites. (A) Representative immunostaining of γ-H2A.X in white matter of tissue sections from residents of MMC and low polluted areas as a control. Scale bar: 20 μm. (B) Quantification of reciprocal intensity of γ-H2A.X staining in white matter nuclei from each individual control and MMC sample is indicated along with mean ± SEM. *p = 0.008, Mann-Whitney *U* test (control: N = 10 subjects; MMC: N = 13 subjects). (C) Representative nuclei positive for γ-H2A.X staining categorized as "light", "medium" or "dark" based on the reciprocal intensity value, which correlates with the amount of chromogen present in the sample (light: 0–49; medium: 50–99; dark: 100–150). (D) Percentage of white matter nuclei of subjects in each of the categories described in C, or with "no staining" (NS) which was added to the percentage of "light" staining. *p = 0.03 (light/NS), *p = 0.02 (dark), MMC versus control, Mann-Whitney *U* test (control: N = 10 subjects; MMC: N = 13 subjects).

In somatic mammalian cells, immunostaining and ChIP assays have shown that the bulk of H3K9me3 is associated with pericentric cHC regions (Lehnertz et al., 2003; Peters et al., 2003; Saksouk et al., 2015). Our observations in mouse cortical neurons showing that H3K9me3 foci co-localize with chromocenters demonstrate that H3K9me3 is associated with satellite repeat sequences within pericentric cHC regions (Lehnertz et al., 2003; Peters et al., 2003; Saksouk et al., 2015). In human brain cells, the clustered distribution of H3K9me3 also suggests that this repressive mark is associated with pericentric satellite repeat sequences. Our observation that H3K9me2 was concentrated in smaller and blurrier foci that did not co-localize with chromocenters is in agreement with the finding that H3K9me2 is enriched at minor satellites of centromeric regions (Allis and Jenuwein, 2016; Peters et al., 2001; Saksouk et al., 2015; Trojer and Reinberg, 2007; Zheng et al., 2019). Critically, we found that H3K9me2/me3 staining was reduced in the cortex of humans and mice exposed to ambient urban particulate air pollution. Similar quantitative single-cell imaging studies of neurons in tissue derived from AD patients and tau models of AD have also found strongly reduced staining of H3K9me3 (Mansuroglu et al., 2016) and H3K9me2 (Frost et al., 2014). Neuropathological hallmarks of AD - including hyperphosphorylated tau and Aβ plaques - are evolving in MMC infants, children and young adults, and significant cognitive impairment is evident in 55% of the young adult cohorts age 21.60 ± 5.88 years with exposures of $PM_{2.5}$ above USA EPA policy limits (Calderón-Garciduñas et al., 2008b, 2012, 2019; Thal et al., 2002). As shown here, young mice exposed to $PM_{2.5}$ above USA EPA standards in Santiago have higher AT8 tau phosphorylation. These observations strongly suggest that loss of H3K9me2/me3 could play a role in the development and progression of neurodegenerative

processes and the resultant cognitive impairment in young urbanites exposed to fine and ultrafine particulate air pollution. Although we were not able to determine cell-type specific changes in HPTMs in the white matter, due to the very low number of neuronal nuclei present in this region (Fig. S7), it is likely that epigenetic changes are occurring in glial and/or endothelial cells. Interestingly, white matter degeneration is an early abnormality observed in AD, that is associated with loss of myelin and myelinated axons, oligodendrocytes dysfunction, increased activation of astrocytes, and microvascular abnormalities (de la Monte and Grammas, 2019). Thus, the epigenetic changes observed in pollution-exposed subjects, could promote white matter dysfunction and contribute to the progression of neurodegenerative processes.

Mechanisms that could be responsible for loss of H3K9me2/me3 include decreased expression of H3K9 methyltransferases and/or increased expression of H3K9 demethylases, and/or oxidative stress. In *Drosophila*, oxidative stress can cause DNA damage and reduce H3K9me2 levels (Frost et al., 2014). A key potential culprit for increased oxidative stress in pollution-exposed humans is the abundance of rounded, electrodense NPs, including iron-rich NPs, observed here in the frontal cortex. The presence of ~10^9 ferrimagnetic NPs/g tissue (dry weight) indicates the high potential for redox activity associated with such Fe- (and, specifically Fe^{2+}-) rich NPs, which are abundant in urban airborne pollution. If redox-active ferrous (Fe^{2+}) remains unbound and freely available in the brain, it can catalyze the formation of reactive oxygen species, including the damaging hydroxyl radical (HO·), through the Fenton reaction (Maher, 2019; Shuster-Meiseles et al., 2016). Also, airborne iron-rich and magnetic NPs are often associated both with other transition metal-bearing NPs and surface-adsorbed organic compounds, including polyaromatic hydrocarbons, such
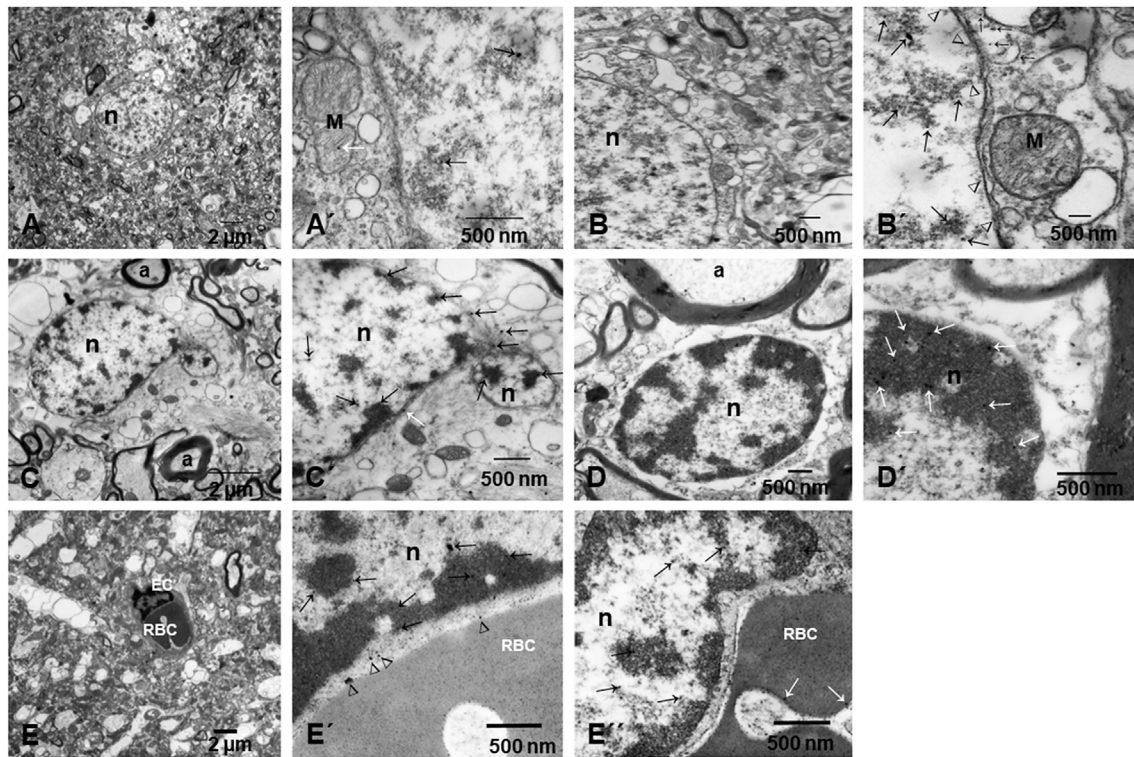
Fig. 4. TEM analysis in frontal cortex of control and MMC subjects. (A-A′) Nucleus (n) of a frontal cortex neuron from a control subject at 5,000x (A) and 15,000x (A′) magnification. Black arrows indicate intranuclear, likely metal-rich NPs. A white arrow shows one single NP inside a mitochondrion (M). (B–B′) Nucleus of a frontal cortex neuron from an MMC urbanite at 5,000x (B) and 80,000x (B′) magnification. Long black arrows indicate intranuclear NPs. White arrowheads indicate CFDNPs in the proximity of the nuclear lipid bilayer and short black arrows indicate rounded, electrodense NPs in the cytoplasm. A mitochondrion is marked (M). (C–C′) Nucleus of a frontal astrocyte from an MMC subject at 12,000x (C) and 20,000x (C′) magnification. Nucleus (n) and myelinated axons (a) are marked. In C′, black arrows indicate intranuclear and intracytoplasmic NPs and the single white arrow shows one NP in between the inner and outer nuclear membranes. (D-D′) Nucleus of an oligodendroglial cell in the frontal cortex from an MMC subject at 20,000x (D) and 50,000x (D′) magnification. D shows the oligodendroglia nucleus (n) and one myelinated axon (a). D′ white arrows indicate numerous rounded, electrodense NPs in close contact with chromatin. (E-E′′) Frontal capillary in a MMC resident containing a luminal red blood cell (RBC) at 5,000x (E) and 50,000x (E′-E′′) magnification. (E′) Micrograph shows the endothelial cell (EC) nucleus with numerous NPs of variable sizes (black arrows); the white arrowheads show NPs in the EC cytoplasm. (E′′) RBC with numerous NPs. The EC nucleus (n) has numerous NPs (black arrows).

as the known carcinogen benzo[*a*]pyrene (Maher, 2019).

The functional consequences of reduced H3K9me2/me3 levels in brain cells could result in abnormal gene activation, since profiling studies have implicated H3K9me2/me3 in the transcriptional silencing of coding genes in both fHC and active euchromatic regions (Bannister and Kouzarides, 2011; Bustos et al., 2017; Regha et al., 2007; Zeller et al., 2016). Moreover, we observed an increase in the active transcription marks H3K4me3 and H3K36me3 in MMC frontal brain tissue samples, supporting abnormal gene activation. In agreement with this notion, microarray and qRT-PCR assays of autopsy samples of the frontal cortex from control and MMC pollution-exposed children and young adults revealed an upregulation (>2 fold) of 134 coding genes in oxidative stress, DNA damage signaling, inflammation, and neurodegeneration pathways (Calderón-Garcidueñas et al., 2012). Loss of H3K9me2/me3 levels at cHC regions could also have important negative consequences as has become evident from H3K9 methyl transferases KO studies. Thus, Suv39h-deficient mice displayed severely impaired viability, chromosomal instability (presence of hyper-tetraploid number of chromosomes), and higher levels of major (but not minor) satellite repeat transcripts underlying pericentromeric cHC regions (Lehnertz et al., 2003; Peters et al., 2001). Several additional reports using rodents have detected chromosome instability and elevated levels of RNA from major satellite repeats and LINE elements upon loss of H3K9 methyl transferases, including SETDB1, SUV39 isoforms, or G9a and GLP (Dodge et al., 2004; Saksouk et al., 2015; Shinkai and Tachibana, 2011). Importantly, evidence for heterochromatin relaxation, aberrant expression of genes and transposable

elements has been found in patients and tau animal models of AD (Frost et al., 2014; Sun et al., 2018), shown to have reduced H3K9me3 (Mansuroglu et al., 2016) and H3K9me2 staining (Frost et al., 2014). Together, these results indicate that reduced H3K9me2/me3 in mice and humans exposed to particulate air pollution could result in a more "relaxed" heterochromatin organization, prone to de-repression of genes and repetitive elements, chromosome instability and DNA damage. In accordance to the latter, we observed an increase in the staining of γ-H2A.X, a widely used marker of DSBs and DNA damage (Ivashkevich et al., 2012; Kinner et al., 2008), in the white matter of urbanites exposed to air pollution and in the frontal cortex of mice exposed to particulate air pollution.

It is noteworthy that the annual mean $PM_{2.5}$ levels in both MMC and Santiago are considerably lower than those in countries such as China and India, which exceed by $\sim$ 4-5-fold the WHO annual $PM_{2.5}$ guideline of 10 µg m^{-3} (Cohen et al., 2017; WHO, 2005), potentially predisposing more deleterious brain defects in urbanites living in these countries. Our findings show that the presence of NPs in the nuclei of brain cells is associated with impaired chromatin silencing and reduced DNA integrity. Critically, these small particles contribute very little to measured $PM_{2.5}$ mass concentrations but dominate in particle number. Thus, specific monitoring and regulation of such UFPs becomes imperative and urgent.
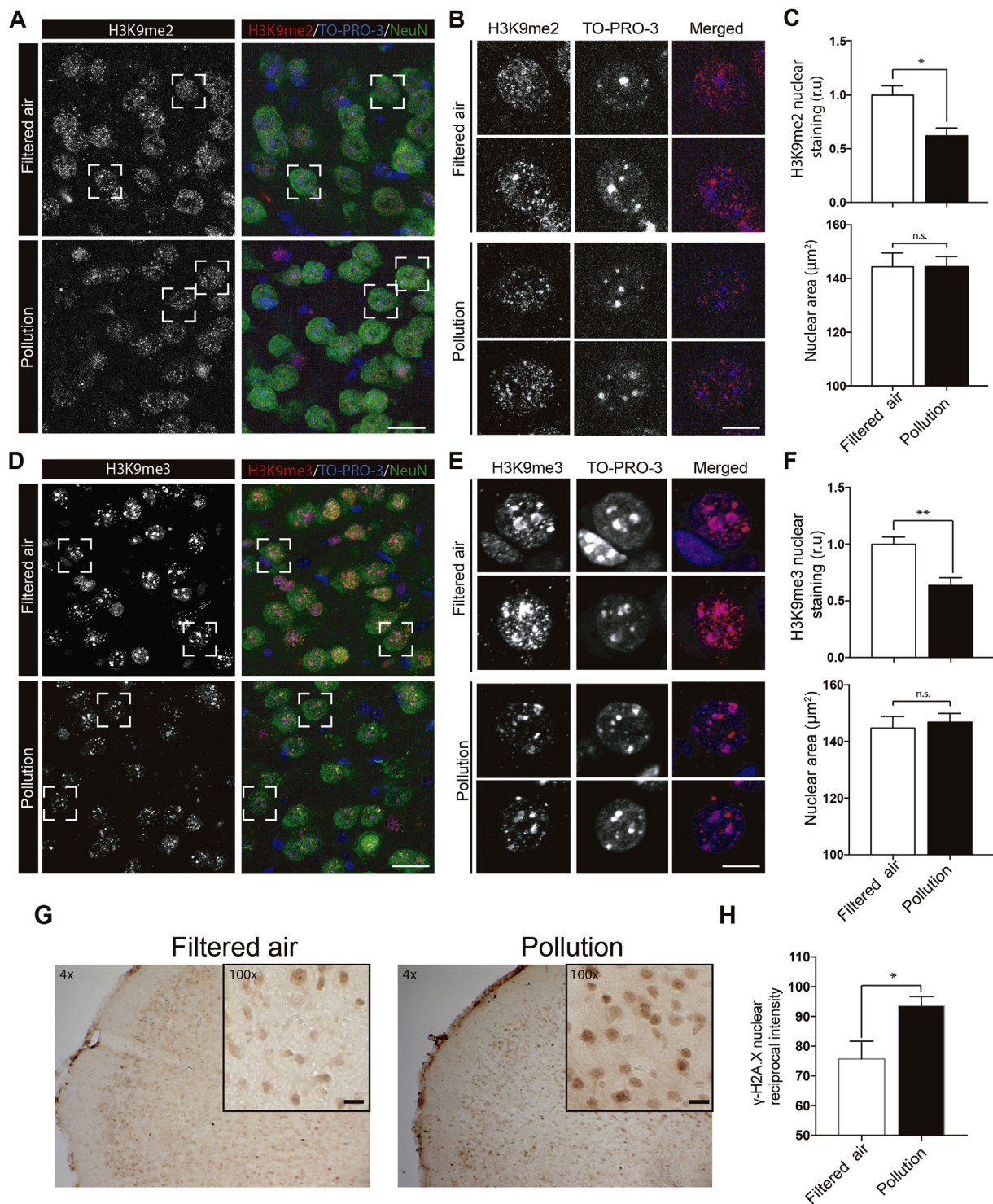
Fig. 5. Immunodetection of H3K9me2/me3 and γ-H2A.X in frontal cortex of mice chronically exposed to particulate air pollution. (A–F) Representative immuno-fluorescence staining of H3K9me2 (A) or H3K9me3 (D) in prefrontal cortex tissue sections from mice exposed to ambient air (pollution group) or to HEPA-filtered air (filtered control group) for 7 months. Scale bar: 20 μm. (B, E) Representative nuclei analyzed in A and D, which are co-stained with the neuronal marker NeuN and the nuclear staining TO-PRO-3. Scale bar: 10 μm. Note that H3K9me3, unlike H3K9me2, displays a prominent perinuclear and perinucleolar staining that co-localizes with TO-PRO-3-chromocenters. (C, F) Top, quantification of nuclear intensity of H3K9me2 (C) or H3K9me3 (F). Values are expressed relative to the control group (relative units, r.u.). Bottom, quantification of the area of nuclei analyzed. Bars represent mean ± SEM. *p = 0.0159; **p = 0.0079; ns, not statistically different (p = 0.6949 (C), p = 0.9768 (F)); Student's t-test (N = 4 mice per group). (G) Representative immunohistochemical staining of γ-H2A.X in frontal cortex tissue sections from mice exposed to pollution or filtered air as a control (insets scale bar: 20 μm). (H) Quantification of reciprocal intensity of γ-H2A.X staining in frontal cortex nuclei from control and pollution groups is indicated. Bars represent mean ± SEM. *p = 0.0368, Student's t-test (N = 4 mice per group).
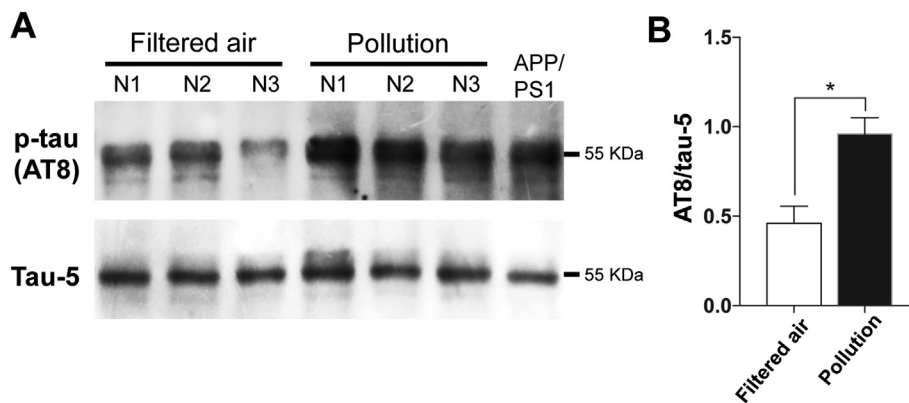
Fig. 6. Tau phosphorylation in the cortex of mice chronically exposed to particulate air pollution. (A) Immunoblot analysis showing immunoreactivity to AT8 (phosphorylated tau) and Tau5 (total tau) in total protein extracts from cortex from mice exposed to ambient air (pollution group) or to HEPA-filtered air for 7 months. Protein extract from hippocampus of 12 month-old double transgenic APPswe-PS1ΔE9 (APP/PS1) mice was used a positive control. (B) Quantification of AT8 to Tau5 immunoreactivity ratio. *p = 0.0194, Student's t-test (N = 3 mice per group).

Appendix A. Supplementary data

Supplementary data to this article can be found online at https://doi.org/10.1016/j.envres.2020.109226.

References

Alegria-Torres, J.A., Baccarelli, A., Bollati, V., 2011. Epigenetics and lifestyle. Epigenomics 3, 267–277.

Allis, C.D., Jenuwein, T., 2016. The molecular hallmarks of epigenetic control. Nat. Rev. Genet. 17, 487–500.

Bannister, A.J., Kouzarides, T., 2011. Regulation of chromatin by histone modifications. Cell Res. 21, 381–395.

Berson, A., Nativio, R., Berger, S.L., Bonini, N.M., 2018. Epigenetic regulation in neurodegenerative diseases. Trends Neurosci. 41, 587–598.

Braak, H., Thal, D.R., Ghebremedhin, E., Del Tredici, K., 2011. Stages of the pathologic process in alzheimer disease: age categories from 1 to 100 years. J. Neuropathol. Exp. Neurol. 70, 960–969.

Braak, H., Del Tredici, K., 2015. The preclinical phase of the pathological process underlying sporadic alzheimer's disease. Brain 138, 2814–2833.

Bustos, F.J., Ampuero, E., Jury, N., Aguilar, R., Falahi, F., Toledo, J., et al., 2017. Epigenetic editing of the dlg4/psd95 gene improves cognition in aged and alzheimer's disease mice. Brain 140, 3252–3268.

Calderón-Garcidueñas, L., Reed, W., Maronpot, R.R., Henriquez-Roldan, C., Delgado-Chavez, R., Calderon-Garciduenas, A., et al., 2004. Brain inflammation and alzheimer's-like pathology in individuals exposed to severe air pollution. Toxicol. Pathol. 32, 650–658.

Calderón-Garcidueñas, L., Mora-Tiscareno, A., Ontiveros, E., Gomez-Garza, G., Barragan-Mejia, G., Broadway, J., et al., 2008a. Air pollution, cognitive deficits and brain abnormalities: a pilot study with children and dogs. Brain Cognit. 68, 117–127.

Calderón-Garcidueñas, L., Solt, A.C., Henriquez-Roldan, C., Torres-Jardon, R., Nuse, B., Herritt, L., et al., 2008b. Long-term air pollution exposure is associated with neuroinflammation, an altered innate immune response, disruption of the blood-brain barrier, ultrafine particulate deposition, and accumulation of amyloid beta-42 and alpha-synuclein in children and young adults. Toxicol. Pathol. 36, 289–310.

Calderón-Garcidueñas, L., Kavanaugh, M., Block, M., D'Angiulli, A., Delgado-Chavez, R., Torres-Jardon, R., et al., 2012. Neuroinflammation, hyperphosphorylated tau, diffuse amyloid plaques, and down-regulation of the cellular prion protein in air pollution exposed children and young adults. J. Alzheim. Dis. 28, 93–107.

Calderón-Garcidueñas, L., Reynoso-Robles, R., Vargas-Martinez, J., Gomez-Maqueo-Chew, A., Perez-Guille, B., Mukherjee, P.S., et al., 2016. Prefrontal white matter pathology in air pollution exposed Mexico city young urbanites and their potential impact on neurovascular unit dysfunction and the development of alzheimer's disease. Environ. Res. 146, 404–417.

Calderón-Garcidueñas, L., Gonzalez-Maciel, A., Reynoso-Robles, R., Delgado-Chavez, R., Mukherjee, P.S., Kulesza, R.J., et al., 2018. Hallmarks of alzheimer disease are evolving relentlessly in metropolitan Mexico city infants, children and young adults. Apoe4 carriers have higher suicide risk and higher odds of reaching nft stage v at < / = 40 years of age. Environ. Res. 164, 475–487.

Calderón-Garcidueñas, L., Mukherjee, P.S., Kulesza, R.J., Torres-Jardon, R., Hernandez-Luna, J., Avila-Cervantes, R., et al., 2019. Mild cognitive impairment and dementia involving multiple cognitive domains in mexican urbanites. J. Alzheim. Dis. 68, 1113–1123.

Chen, H., Kwong, J.C., Copes, R., Hystad, P., van Donkelaar, A., Tu, K., et al., 2017a. Exposure to ambient air pollution and the incidence of dementia: a population-based cohort study. Environ. Int. 108, 271–277.

Chen, H., Kwong, J.C., Copes, R., Tu, K., Villeneuve, P.J., van Donkelaar, A., et al., 2017b. Living near major roads and the incidence of dementia, Parkinson's disease, and multiple sclerosis: a population-based cohort study. Lancet 389, 718–726.

Cohen, A.J., Brauer, M., Burnett, R., Anderson, H.R., Frostad, J., Estep, K., et al., 2017. Estimates and 25-year trends of the global burden of disease attributable to ambient air pollution: an analysis of data from the global burden of diseases study 2015. Lancet 389, 1907–1918.

de la Monte, S.M., Grammas, P., 2019. Insulin resistance and oligodendrocyte/microvascular endothelial cell dysfunction as mediators of white matter degeneration in Alzheimer's disease. In: Wisniewski, T. (Ed.), Alzheimer's Disease, Brisbane (AU).

Dodge, J.E., Kang, Y.K., Beppu, H., Lei, H., Li, E., 2004. Histone h3-k9 methyltransferase eset is essential for early development. Mol. Cell Biol. 24, 2478–2486.

Dumbovic, G., Forcales, S.V., Perucho, M., 2017. Emerging roles of macrosatellite repeats in genome organization and disease development. Epigenetics 12, 515–526.

Forns, J., Dadvand, P., Esnaola, M., Alvarez-Pedrerol, M., Lopez-Vicente, M., Garcia-Esteban, R., et al., 2017. Longitudinal association between air pollution exposure at school and cognitive development in school children over a period of 3.5 years. Environ. Res. 159, 416–421.

Frost, B., Hemberg, M., Lewis, J., Feany, M.B., 2014. Tau promotes neurodegeneration through global chromatin relaxation. Nat. Neurosci. 17, 357–366.

Goedert, M., Jakes, R., Vanmechelen, E., 1995. Monoclonal antibody at8 recognises tau protein phosphorylated at both serine 202 and threonine 205. Neurosci. Lett. 189, 167–169.

Gonet, T., Maher, B.A., 2019. Airborne, vehicle-derived fe-bearing nanoparticles in the urban environment – a review. Environ. Sci. Technol. 53, 9970–9991.

Graff, J., Tsai, L.H., 2013. Histone acetylation: molecular mnemonics on the chromatin. Nat. Rev. Neurosci. 14, 97–111.

Harr, J.C., Gonzalez-Sandoval, A., Gasser, S.M., 2016. Histones and histone modifications in perinuclear chromatin anchoring: from yeast to man. EMBO Rep. 17, 139–155.

Harris, M.H., Gold, D.R., Rifas-Shiman, S.L., Melly, S.J., Zanobetti, A., Coull, B.A., et al., 2015. Prenatal and childhood traffic-related pollution exposure and childhood cognition in the project viva cohort (Massachusetts, USA). Environ. Health Perspect. 123, 1072–1078.

Ivashkevich, A., Redon, C.E., Nakamura, A.J., Martin, R.F., Martin, O.A., 2012. Use of the gamma-h2ax assay to monitor DNA damage and repair in translational cancer research. Canc. Lett. 327, 123–133.

Jorquera, H., Barraza, F., 2012. Source apportionment of ambient pm2.5 in santiago, Chile: 1999 and 2004 results. Sci. Total Environ. 435–436, 418–429.

Jung, C.R., Lin, Y.T., Hwang, B.F., 2015. Ozone, particulate matter, and newly diagnosed alzheimer's disease: a population-based cohort study in taiwan. J. Alzheim. Dis. 44, 573–584.

Kinner, A., Wu, W., Staudt, C., Iliakis, G., 2008. Gamma-h2ax in recognition and signaling of DNA double-strand breaks in the context of chromatin. Nucleic Acids Res. 36, 5678–5694.

Klein, H.U., McCabe, C., Gjoneska, E., Sullivan, S.E., Kaskow, B.J., Tang, A., et al., 2019. Epigenome-wide study uncovers large-scale changes in histone acetylation driven by tau pathology in aging and alzheimer's human brains. Nat. Neurosci. 22, 37–46.

Lehnertz, B., Ueda, Y., Derijck, A.A., Braunschweig, U., Perez-Burgos, L., Kubicek, S., et al., 2003. Suv39h-mediated histone h3 lysine 9 methylation directs DNA methylation to major satellite repeats at pericentric heterochromatin. Curr. Biol. 13, 1192–1200.

Li, R., Zhou, R., Zhang, J., 2018. Function of pm2.5 in the pathogenesis of lung cancer and chronic airway inflammatory diseases. Oncol. Lett. 15, 7506–7514.

Maher, B.A., 1988. Magnetic properties of some synthetic sub-micron magnetites. Geophys. J. Int. 94, 83–96.

Maher, B.A., Ahmed, I.A., Karloukovski, V., MacLaren, D.A., Foulds, P.G., Allsop, D., et al., 2016. Magnetite pollution nanoparticles in the human brain. Proc. Natl. Acad. Sci. U. S. A. 113, 10797–10801.

Maher, B.A., 2019. Airborne magnetite- and iron-rich pollution nanoparticles: potential neurotoxicants and environmental risk factors for neurodegenerative disease, including alzheimer's disease. J. Alzheim. Dis. 71, 361–375.

Mansuroglu, Z., Benhelli-Mokrani, H., Marcato, V., Sultan, A., Violet, M., Chauderlier, A., et al., 2016. Loss of tau protein affects the structure, transcription and repair of neuronal pericentromeric heterochromatin. Sci. Rep. 6, 33047.

Mikkelsen, T.S., Ku, M., Jaffe, D.B., Issac, B., Lieberman, E., Giannoukos, G., et al., 2007.

Genome-wide maps of chromatin state in pluripotent and lineage-committed cells. Nature 448, 553–560.

Nguyen, D.H., Zhou, T., Shu, J., Mao, J.H., 2013. Quantifying chromogen intensity in immunohistochemistry via reciprocal intensity. Canc. InCytes 2.

Perera, F.P., Rauh, V., Whyatt, R.M., Tsai, W.Y., Tang, D., Diaz, D., et al., 2006. Effect of prenatal exposure to airborne polycyclic aromatic hydrocarbons on neurodevelopment in the first 3 years of life among inner-city children. Environ. Health Perspect. 114, 1287–1292.

Peters, A.H., O'Carroll, D., Scherthan, H., Mechtler, K., Sauer, S., Schofer, C., et al., 2001. Loss of the suv39h histone methyltransferases impairs mammalian heterochromatin and genome stability. Cell 107, 323–337.

Peters, A.H., Kubicek, S., Mechtler, K., O'Sullivan, R.J., Derijck, A.A., Perez-Burgos, L., et al., 2003. Partitioning and plasticity of repressive histone methylation states in mammalian chromatin. Mol. Cell. 12, 1577–1589.

Prieto-Parra, L., Yohannessen, K., Brea, C., Vidal, D., Ubilla, C.A., Ruiz-Rudolph, P., 2017. Air pollution, pm2.5 composition, source factors, and respiratory symptoms in asthmatic and nonasthmatic children in santiago, Chile. Environ. Int. 101, 190–200.

Querol, X., Pey, J., Minguillón, M.C., Pérez, N., Alastuey, A., Viana, M., et al., 2008. Pm speciation and sources in Mexico during the milagro-2006 campaign. Atmos. Chem. Phys. 8, 111–128.

Regha, K., Sloane, M.A., Huang, R., Pauler, F.M., Warczok, K.E., Melikant, B., et al., 2007. Active and repressive chromatin are interspersed without spreading in an imprinted gene cluster in the mammalian genome. Mol. Cell. 27, 353–366.

Rogakou, E.P., Boon, C., Redon, C., Bonner, W.M., 1999. Megabase chromatin domains involved in DNA double-strand breaks in vivo. J. Cell Biol. 146, 905–916.

Rothkamm, K., Lobrich, M., 2003. Evidence for a lack of DNA double-strand break repair in human cells exposed to very low x-ray doses. Proc. Natl. Acad. Sci. U. S. A. 100, 5057–5062.

Ruthenburg, A.J., Allis, C.D., Wysocka, J., 2007. Methylation of lysine 4 on histone h3: intricacy of writing and reading a single epigenetic mark. Mol. Cell. 25, 15–30.

Saksouk, N., Simboeck, E., Dejardin, J., 2015. Constitutive heterochromatin formation and transcription in mammals. Epigenet. Chromatin 8, 3.

Sedelnikova, O.A., Rogakou, E.P., Panyutin, I.G., Bonner, W.M., 2002. Quantitative detection of (125)idu-induced DNA double-strand breaks with gamma-h2ax antibody. Radiat. Res. 158, 486–492.

Shinkai, Y., Tachibana, M., 2011. H3k9 methyltransferase g9a and the related molecule glp. Genes Dev. 25, 781–788.

Shuster-Meiseles, T., Shafer, M.M., Heo, J., Pardo, M., Antkiewicz, D.S., Schauer, J.J., et al., 2016. Ros-generating/are-activating capacity of metals in roadway particulate matter deposited in urban environment. Environ. Res. 146, 252–262.

Suarez, L., Mesias, S., Iglesias, V., Silva, C., Caceres, D.D., Ruiz-Rudolph, P., 2014. Personal exposure to particulate matter in commuters using different transport modes (bus, bicycle, car and subway) in an assigned route in downtown santiago, Chile. Environ. Sci. Process Impact. 16, 1309–1317.

Suglia, S.F., Gryparis, A., Wright, R.O., Schwartz, J., Wright, R.J., 2008. Association of black carbon with cognition among children in a prospective birth cohort study. Am. J. Epidemiol. 167, 280–286.

Sun, W., Samimi, H., Gamez, M., Zare, H., Frost, B., 2018. Pathogenic tau-induced pirna depletion promotes neuronal death through transposable element dysregulation in neurodegenerative tauopathies. Nat. Neurosci. 21, 1038–1048.

Thal, D.R., Rub, U., Orantes, M., Braak, H., 2002. Phases of a beta-deposition in the human brain and its relevance for the development of ad. Neurology 58, 1791–1800.

Trojer, P., Reinberg, D., 2007. Facultative heterochromatin: is there a distinctive molecular signature? Mol. Cell. 28, 1–13.

Vecoli, C., Pulignani, S., Andreassi, M.G., 2016. Genetic and epigenetic mechanisms linking air pollution and congenital heart disease. J. Cardiovasc. Dev. Dis. 3.

Weichenthal, S., Olaniyan, T., Christidis, T., Lavigne, E., Hatzopoulou, M., Van Ryswyk, K., et al., 2019. Within-city Spatial Variations in Ambient Ultrafine Particle Concentrations and Incident Brain Tumors in Adults. Epidemiology In press.

WHO, 2005. Air Quality Guidelines- Global Update. Copenhagen. World Health Organization Regional Office for Europe.

Yang, I.V., Lozupone, C.A., Schwartz, D.A., 2017. The environment, epigenome, and asthma. J. Allergy Clin. Immunol. 140, 14–23.

Zeller, P., Padeken, J., van Schendel, R., Kalck, V., Tijsterman, M., Gasser, S.M., 2016. Histone h3k9 methylation is dispensable for caenorhabditis elegans development but suppresses rna:DNA hybrid-associated repeat instability. Nat. Genet. 48, 1385–1395.

Zeller, P., Gasser, S.M., 2017. The importance of satellite sequence repression for genome stability. Cold Spring Harbor Symp. Quant. Biol. 82, 15–24.

Zhang, X., Chen, X., Zhang, X., 2018. The impact of exposure to air pollution on cognitive performance. Proc. Natl. Acad. Sci. U. S. A. 115, 9193–9197.

Zheng, Y., Liu, A., Wang, Z.J., Cao, Q., Wang, W., Lin, L., et al., 2019. Inhibition of ehmt1/2 rescues synaptic and cognitive functions for alzheimer's disease. Brain 142, 787–807.